Modulated metasurface array for photonic beam steering at W band

Jérôme Taillieu, Ronan Sauleau, Mehdi Alouini, David Gonzalez-Ovejero

Modulated metasurface array for photonic beam steering at W band

Jérôme Taillieu[1,2], Ronan Sauleau[1], Mehdi Alouini[2], David González Ovejero[1]
[1] Univ Rennes, CNRS, IETR (Institut d'Électronique et des Technologies du numéRique) – UMR 61614, F-35000, Rennes, France, jerome.taillieu@univ-rennes1.fr *
[2] Univ Rennes, CNRS, Institut FOTON – UMR 6082, F-35000 Rennes, France

***Abstract*— This contribution presents a photonically excited modulated metasurface array, which enables one dimensional beam steering with a medium-to-high gain in the sub-THz range. The designed array consists of four rectangular sub-arrays separated $1.16\times\lambda_0$, with λ_0 being the free-space wavelength at 100 GHz. This spacing permits a scanning range of +/-5° without grating lobes. The sub-arrays radiate at broadside and are excited at their center by a simple substrate integrated waveguide (SIW) circuit. The excitation consists in a Uni-Traveling-Carrier photodiodes (UTC-PD) connected to a wideband DC biasing network. The structure at hand exhibits 26 dB of gain with a 3% relative gain bandwidth, enables power-combining and it is easily scalable for higher gains.**

***Index Terms*— beam-steering, mm-Wave, modulated metasurface, photonic transmitter, UTC photodiode, W-band.**

I. INTRODUCTION

By the end of 2030, wireless data rates beyond 1 Tera-bit/s will be requested [1], and a more efficient use of the allocated frequency bands will not suffice to satisfy this demand. The use of millimeter waves (mm-waves) will be essential to reach the predicted data rates, so new technologies must be developed to enable an efficient and reliable network. Microwave photonics has sprung up as a very promising technology for high data-rates wireless communications at mm-waves and beyond [2].

For back-hauling applications, a realistic link of 100 m must compensate a free space path loss (FSPL) as high as 110 dB [3]. Nonetheless, state-of-the-art high frequency photodiodes are able to produce (in optimal conditions) only 10 dBm of RF power at 100 GHz. Therefore, a large fraction of the available power must be transmitted towards the desired direction to provide a good quality of service (QoS) [4]. This is the reason why high gain (> 25 dB) antennas with beam scanning over a narrow field of view (< 10°) are compulsory to guarantee that the links are resilient to beam misalignment [5]. However, active phased arrays at sub-THz frequencies are costly and technologically challenging. Thus, well-established photonic technologies with wideband performance and a high integration level constitute an interesting alternative for efficient beam forming networks.

A photonic mm-wave transmitter comprises, at least, two elements: 1) An opto-electronic converter such as a fast photodiode (PIN, UTC-PD) that down converts the signal from optical-to-RF domain, and 2) an antenna. These two elements can be placed on a single chip at the expense of strict design constraints and the detrimental excitation of surface waves (SWs) on the high permittivity semiconductor substrate. A promising alternative consists in using a hybrid approach with the down-conversion device connected to the antenna on a printed circuit board (PCB). The photonic approach has several key benefits. Firstly, it takes advantage of cost-effective photonic components for optical telecommunications, such as: amplifiers, wideband modulators, and a variety of fiber-based components. Secondly, it significantly simplifies and miniaturizes the active beamforming network by utilizing optical true-time-delay lines or phase shifters with integrated photonics circuits. In this paper, we propose a wideband opto-electronic transition connected to a scalable modulated metasurface (MTS) sub-array capable of 1D beam-steering over a limited field of view for self-alignment in back-hauling applications. Since each sub-array is excited by a UTC-PD, we also benefit from power combining, thus obtaining higher levels of radiated power.

II. ANTENNA ARRAY ELEMENTS

A. Wideband opto-electronic biasing transition

This transition can be used to feed multiple types of antenna structures, from single layer PCB to more complex stack-ups [6], [7]. It is designed on a 254um thick Astra® MT77 ($\varepsilon r = 3.0 \pm 0.1$, $\tan\delta = 0.0015 \pm 0.0005$ up to 100 GHz). The substrate has been chosen sufficiently thick to provide a stiff structure that does not bend and breaks the bonding with the UTC-PDs, and thin enough to avoid the excitation of SWs. The substrate thickness also plays a role in the vertical coupling to the substrates below. The available chips comprise two closely spaced photodiodes, as shown in [8]. They are mounted on an Aluminum Nitride carrier (AlN) to ensure thermal dissipation of the high optical power injected through their input optical waveguide. The co-planar waveguides (CPW) of the UTC-PD chip are connected to the PCB using conductive silver filled epoxy, since thin gold wires may induce losses as high as -9dB [9]. On the PCB side, grounded co-planar waveguides (GCPW) are adopted to minimize loses, the excitation of unwanted SWs and the coupling between closely spaced lines.

The line impedance of the input GCPW on the PCB is 76 Ω. This choice is driven by the pitch between the UTC-PD in the available chips, which dictates the maximum width of the GCPW. The GCPW line is then linearly tapered to reach a line impedance of 50 Ω. It is important to note that the UTC-PDs must be polarized to evacuate the electrons faster and reduce the parasitic capacitance, while remaining transparent to the RF signal. At W band, the width of the signal line in a 50 Ω GCPW represents an unneglectable fraction of the guided wavelength, which may lead to the excitation of the coupled slotline mode in the bias-Tee's GCPW line. To counteract this effect, the signal line in the RF choke must be as narrow as possible and, thus, one cannot use of ultra-compact split ring resonators (SRRs) as in [10],[11]. The proposed RF choke is composed of a classical butterfly shape dual-stub encaged by wire bonding to avoid undesired spurious radiation (Fig.1). The RF isolation and transmission are shown in Fig. 2. Our transition shows a stable behavior from 60GHz to 120GHz with a high transmission and insertion loss lower than 2dB. Besides, the DC isolation is higher than 15dB.

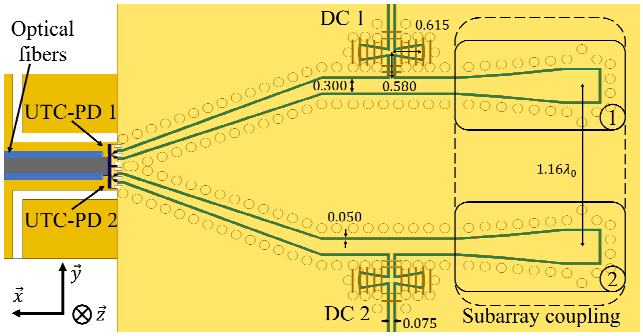

Fig. 1. Top view of the transition from the UTC-PD chip to GCPW. Units in millimeters.

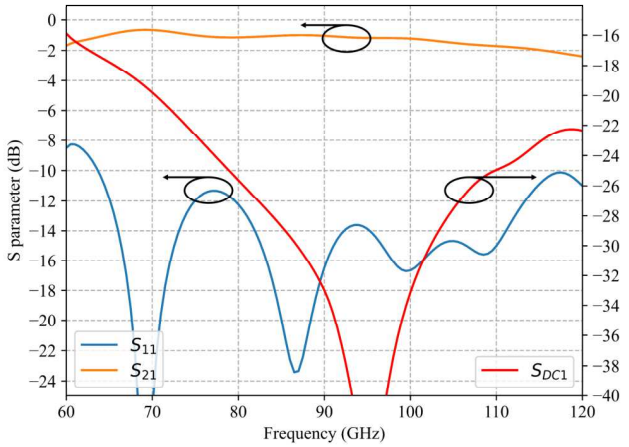

Fig. 2. S Parameter (in dB) of the transition UTC-PDs to GCPW.

B. Modulated Meta-Surface subarray

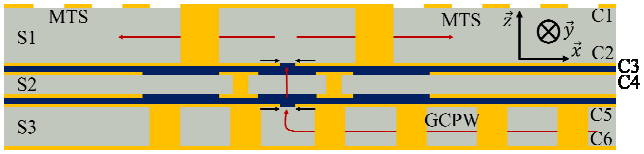

Fig. 3. PCB stack-up and side-view (not to scale) of the designed MTS array. The red lines represent the power flow.

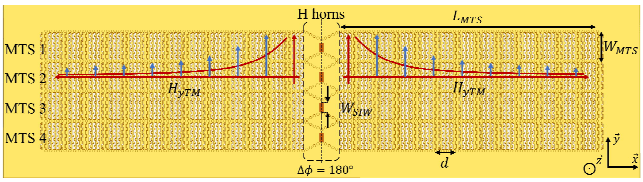

Fig. 4. Top view of the 4 modulated MTS subarrays.

1) Subarray feeding structure

The stack-up of the structure is shown in Fig. 3. It consists of three dielectric layers of Astra® MT77 ($\varepsilon_r = 3.0 \pm 0.1$, $\tan\delta = 0.0015 \pm 0.0005$ up to 100 GHz) glued with prepreg Rogers CuClad 6250 ($\varepsilon_r = 2.32$, $\tan\delta = 0.003$ at 78.5GHz). The transition from the UTC-PDs to the GCPW discussed in Section II.A corresponds to the bottom metallization (C6) of substrate S3 (see Fig. 3). This substrate also includes the coupler from the GCPW line to the upper substrates, as shown on the right-hand side of Fig. 1. This coupling method to the upper substrates allows one to avoid a complex and lossy DC-block [12]. The 127 um thick middle substrate (S2) has the sole role of ensuring a low loss and contactless transition between the substrate S1 and S3 [13]. The output of the feeding structure in substrate S3 (with thickness h=381µm) consists of two short symmetric SIW sections. The MTS elements are etched on the C1 metal layer on substrate S1. Since the etching accuracy is critical in our design, the metallization thickness of all copper layers has been chemically reduced to 9 µm.

2) Modulated MTS array

The radiating part comprises two symmetric modulated MTS apertures with length L_{MTS}=10λ_0 and width W_{MTS}=1.16 λ_0, with λ_0 being the free space wavelength at 100 GHz. The latter width has been chosen to prevent the onset of grating lobes in a scanning range of ±5 degrees with a grating lobe level lower than 10 dB. Both sections are fed out of phase to grant broadside radiation. To that end, the SIW outputs (with width W_{SIW}=1.22mm, highlighted in red on Fig. 4) in S3 are tapered as H-plane horns until reaching the targeted W_{MTS} value. The MTS apertures consist of a capacitive impedance boundary condition, which has been periodically modulated along the x direction, and lays on the grounded substrate. The combined effect of such capacitance and the inductive grounded substrate S3 yields an inductive boundary condition that supports the propagation of a transverse

magnetic (TM) SW. Owing to this periodic modulation, the TM slow wave supported by the MTS structure is gradually radiated. Without loss of generality, the MTS is modeled as an ideal capacitive boundary condition as

$$X_c = X_0\left[1 + M\sin\left(\frac{2\pi}{d}x\right)\right] \quad (1)$$

where X_0=-313 Ω, M=0.8 and d=2.35 mm. Although one could work directly with the non-penetrable (inductive) impedance boundary condition (IBC) [14], the use of the capacitive sheet transition IBC allows one to exert a higher control on the aperture fields [15]. We propose to synthesize the IBC by utilizing a meandered slot configuration (as depicted in Fig. 5) in order to achieve a broader range of sheet capacitance compared to traditional slot structures [14]. In order to respect the hypothesis of being in the homogenization region, the value of a_x has been selected as $d/5$ to be much smaller than the guided wavelength and the modulation period. The width a_y is set at $W_{SIW}/4$ in this case.

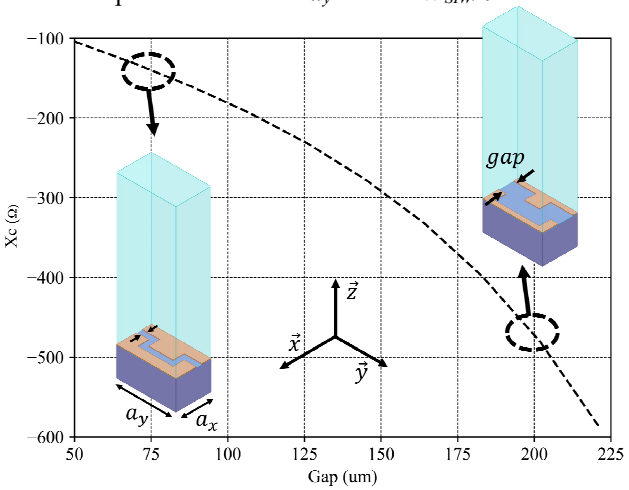

Fig. 5. Relation between the gap of the proposed meandered slot unit-cell and the sheet capacitance at 100GHz.

III. NUMERICAL RESULTS

The E- and H-plane radiation patterns for the structure shown in Fig. 4 are plotted in Figs. 6 and 7, respectively. The scanning is realized in the H plane from -5° to +5° in order to maintain the grating lobes 10dB below from the main lobe. The cross-polarized patterns (not shown here) remain 20dB below the maximum both for the E and H planes.

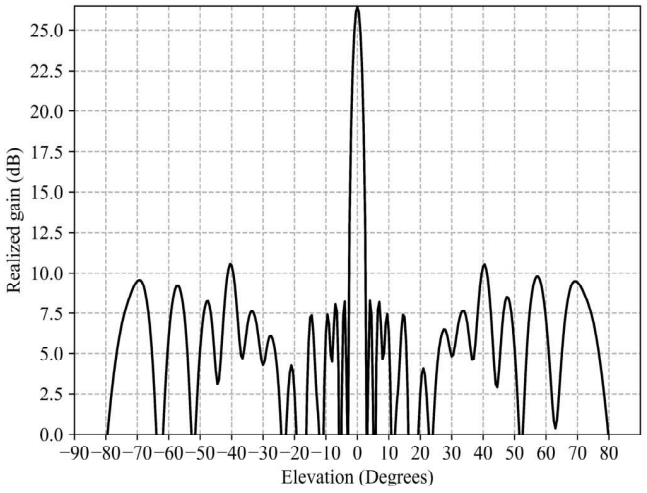

Fig. 6. Realized gain in E plane at 100GHz.

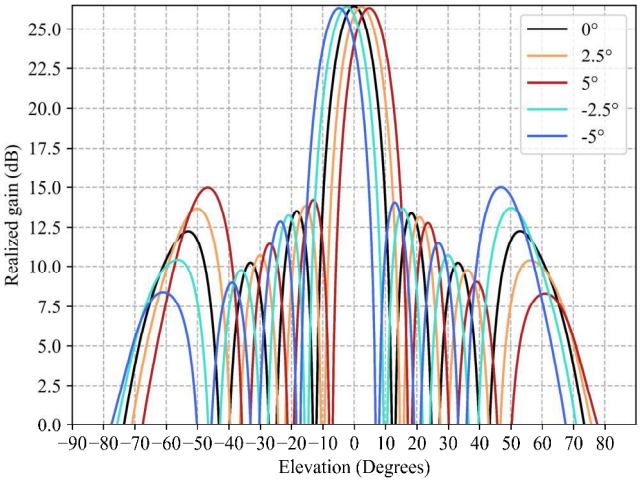

Fig. 7. Realized gain in H plane with steering angles between -5° to 5° at 100GHz.

The calculated -3dB gain bandwidth is 3.6 GHz. The somehow narrow bandwidth is mostly limited by the dispersive nature of the MTS. One can indeed observe a gain drop as the frequency of operation differs from the design frequency. However, it is important to note that larger bandwidths could be obtained by optimizing the local value of the period d in (1), as discussed in [16]. The aperture efficiency reaches 38% at the center frequency, which is a typical value for a modulated metasurface antenna with constant modulation index M [17].

IV. CONCLUSION

This paper has presented the design of a scalable array at W-band. It consists of modulated MTS sub-arrays and is fed by a simple SIW circuit. The array at hand comprises 4 sub-arrays and provides a peak gain of 26.5dB. Moreover, we have described the design of a general-purpose wideband photonic transition covering an octave bandwidth. The array

at hand is compatible with traditional PCB processes and enables photonic beam steering over a 10° scanning range. Moreover, when excited by fast photodiodes, it provides power combining for an increased level of total radiated power in the sub-THz range.

ACKNOWLEDGMENT

The authors would like to thank the European Union through the European Regional Development Fund (ERDF), and the French region of Brittany, Ministry of Higher Education and Research, Rennes Métropole and Conseil Départemental 35, through the CPER Project SOPHIE / STIC & Ondes. This work has received a French government support granted to the Labex CominLabs excellence laboratory and managed by the National Research Agency in the "Investing for the Future" program under reference ANR-10-LABX-07-01.

REFERENCES

[1] T. Huang, W. Yang, J. Wu, J. Ma, X. Zhang, and D. Zhang, "A survey on green 6G network: architecture and technologies," in *IEEE Access*, vol. 7, pp. 175758-175768, 2019.

[2] T. Nagatsuma *et al*., "Millimeter-wave and terahertz-wave applications enabled by photonics," *IEEE J. Quantum Electron.*, vol. 52, no. 1, pp. 1-12, Jan. 2016.

[3] T. Nagatsuma, G. Ducournau, and C. Renaud, "Advances in terahertz communications accelerated by photonics," *Nature Photon.* vol. 10, pp. 371–379, 2016.

[4] T. Nagatsuma, T. Ishibashi, A. Hirata, Y. Hirota, T. Minotani, A. Sasaki, and H. Ito, "Characterisation of uni-travelling-carrier photodiode monolithically integrated with matching circuit," *Electron. Lett.*, vol. 37, no. 20, 1246, 2001.

[5] A. J. Seeds, "Terahertz photonics for communications," *Opt. InfoBase Conf. Pap.*, vol. 33, no. 3, pp. 579–587, 2014.

[6] J. Taillieu, R. Sauleau, M. Alouini, and D. González-Ovejero, "Cavity-backed broadband microstrip antenna array for photonic beam steering at W band," *16th Eur. Conf. Antennas Propag. (EuCAP)*, 2022, pp. 1-5.

[7] A. Lamminen, M. Lahti, D. del Rio, J. Säily, J. F. Sevillano and V. Ermolov, "Characterization of interconnects on multilayer high frequency PCB for D-band," *2nd 6G Wireless Summit (6G SUMMIT)*, 2020, pp. 1-5.

[8] A. J. Pascual *et al*., "A scalable photomixing array for increased emitted power," *2019 44th Int. Conf. Infrared, Millimeter THz Waves (IRMMW-THz)*, 2019, pp. 1-2.

[9] I. Flammia, M. Steeg, A. Jankowski, S. Babiel, V. Rymanov and A. Stohr, Antennas, Wireless and Electromagnetics, *1st IET Colloquium*, 29 May, 2013.

[10] M. Ali, L. E. García Muñoz, and G. Carpintero, "E-band photonic transmitter with tapered slot antenna for RoF applications," *2017 Int. Topical Meeting Microw. Photon. (MWP)*, 2017, pp. 1-4.

[11] M. Palandöken, V. Rymanov, A. Stöhr, and T. Tekin, "Compact metamaterial-based bias tee design for 1.55 m waveguide-photodiode based 71-76 GHz wireless transmitter," *Progress Electromagn. Res. Symp.*, pp. 393-397, 2012.

[12] M. Umar, M. Laabs, N. Neumann, and D. Plettemeier, "Design of DC-blocks and bias-tee on PCB for V-band," *IEEE Microw. Wireless Compon. Lett.*, vol. 31, no. 10, pp. 1107-1110, Oct. 2021.

[13] T. Potelon, M. Ettorre, L. Le Coq, T. Bateman, J. Francey, and R. Sauleau, "Reconfigurable CTS antenna fully integrated in PCB technology for 5G backhaul applications," *IEEE Trans. Antennas Propag.*, vol. 67, no. 6, pp. 3609-3618, Jun. 2019.

[14] A. M. Patel and A. Grbic, "A printed leaky-wave antenna based on a sinusoidally-modulated reactance surface," *IEEE Trans. Antennas Propag.*, vol. 59, no. 6, pp. 2087-2096, Jun. 2011.

[15] J. Ruiz-García, M. Faenzi, A. Mahmoud, M. Ettorre, P. Potier, P. Pouliguen, R. Sauleau, and D. González-Ovejero, "Multi-beam modulated metasurface antenna for 5G backhaul applications at K-band," *Comptes Rendus. Phys.*, Tome 22 (2021) no. S1, pp. 47-52.

[16] M. Faenzi, D. González-Ovejero, and S. Maci, "Wideband active region metasurface antennas," *IEEE Trans. Antennas Propag.*, vol. 68, no. 3, pp. 1261-1272, Mar. 2020.

[17] Enrica Martini; Marco Faenzi; David González-Ovejero; Stefano Maci, "Surface-wave based metasurface antennas, " in *Antenna and Array Technologies for Future Wireless Ecosystems*, IEEE, 2022, pp.1-41.